Extended poromechanics for adsorption-induced swelling prediction in double porosity media: modeling and experimental validation on activated carbon

Laurent Perrier, Gilles Pijaudier-Cabot, David Grégoire

Extended poromechanics for adsorption-induced swelling prediction in double porosity media: modeling and experimental validation on activated carbon

Laurent Perrier, Gilles Pijaudier-Cabot[1], David Grégoire[1,*]

University Pau & Pays Adour,
Laboratoire des Fluides Complexes et leurs Réservoirs, LFCR-IPRA, UMR5150,
Campus Montaury, F-64600 Anglet, France

Abstract

Natural and synthesised porous media are generally composed of a double porosity: a microporosity where the fluid is trapped as an adsorbed phase and a meso or a macro porosity required to ensure the transport of fluids to and from the smaller pores. Zeolites, activated carbon, tight rocks, coal rocks, source rocks, cement paste or construction materials are among these materials.

In nanometer-scale pores, the molecules of fluid are confined. This effect, denoted as molecular packing, induces that fluid-fluid and fluid-solid interactions sum at the pore scale and have significant consequences at the macroscale, such as instantaneous deformation, which are not predicted by classical poromechanics. If adsorption in nanopores induces instantaneous deformation at a higher scale, the matrix swelling may close the transport porosity, reducing the global permeability of the porous system. This is important for applications in petroleum oil and gas recovery, gas storage, separation, catalysis or drug delivery.

This study aims at characterizing the influence of an adsorbed phase on the instantaneous deformation of micro-to-macro porous media presenting distinct and well-separated porosities. A new incremental poromechanical framework with varying porosity is proposed allowing the prediction of the swelling induced by adsorption without any fitting parameters. This model is validated by experimental comparison performed on a high micro and macro porous activated carbon. It is shown also that a single porosity model cannot predict the adsorption-induced strain evolution observed during the experiment. After validation, the double porosity model is used to discuss the evolution of the poromechanical properties under free and constraint swelling.

Keywords: Adsorption, swelling, double porosity media, poromechanical modelling

Introduction

Following the IUPAC recommendation (Sing et al., 1985; Thommes et al., 2015), the pore space in porous materials is divided into three groups according to the pore size diameters: macropores of widths greater than 50 nm, mesopores of widths between 2 and 50 nm and micropores (or nanopores) of widths less than 2 nm. Zeolites, activated carbon, tight rocks, coal rocks, source rocks, cement paste or construction materials are among these materials. In recent years, a major attention has been paid on these microporous materials because the surface-to-volume ratio (i.e., the specific pore surface) increases with decreasing characteristic pore size. Consequently, these materials can trap an important quantity of fluid molecules as an adsorbed phase. This is important for applications in petroleum and oil recovery, gas storage, separation, catalysis or drug delivery.

*Corresponding author: david.gregoire@univ-pau.fr
[1]D. Grégoire and G. Pijaudier-Cabot are fellows of the *Institut Universitaire de France*.

Accepted manuscript in *International Journal of Solids and Structures* (DOI: 10.1016/j.ijsolstr.2018.03.029)
The final publication is available at: https://doi.org/10.1016/j.ijsolstr.2018.03.029 .

For these microporous materials, a deviation from standard poromechanics (Biot, 1941; Coussy, 2004), is expected. In nanometer-scale pores, the molecules of fluid are confined. This effect, denoted as molecular packing, induces that fluid-fluid and fluid-solid interactions sum at the pore scale and have significant consequences at the macroscale, such as instantaneous deformation. A lot of natural and synthesised porous media are composed of a double porosity: the microporosity where the fluid is trapped as an adsorbed phase and a meso or a macro porosity required to ensure the transport of fluids to and from the smaller pores. If adsorption in nanopores induces instantaneous deformation at a higher scale, the matrix swelling may close the transport porosity, reducing the global permeability of the porous system or annihilating the functionality of synthesised materials. In different contexts, this deformation may be critical. For instance, *in situ* adsorption-induced coal swelling has been identified (Larsen, 2004; Pan and Connell, 2007; Sampath et al., 2017) as the principal factor leading to a rapid decrease in CO_2 injectivity during coal bed methane production enhanced by CO_2 injection. Conversely, gas desorption can lead to matrix shrinkage and microcracking, which may help oil and gas recovery in the context of unconventional petroleum engineering (Levine, 1996). The effects of adsorbent deformation on physical adsorption has also been identified by Thommes and Cychosz (2014) as one of the next major challenges concerning gas porosimetry in nano-porous non-rigid materials (e.g. metal organic framework). In conclusion, there is now a consensus in the research community that major attention has to be focused on the coupled effects appearing at the nanoscale within microporous media because they may have significant consequences at the macroscale.

Experimentally, different authors tried to combine gas adsorption results and volumetric swelling data (see e.g. Gor et al. (2017) for a review). The pioneering work of Meehan (1927) showed the effect of carbon dioxyde sorption on the expansion of charcoal but only mechanical deformation was reported and adsorption quantities were not measured. Later on, different authors (Briggs and Sinha, 1933; Levine, 1996; Day et al., 2008; Ottiger et al., 2008; Pini et al., 2009; Hol and Spiers, 2012; Espinoza et al., 2014) performed tests on bituminous coal, because it is of utmost importance in the context of CO_2 geological sequestration and coal bed reservoirs exploitation. However, most results were not complete in a sense that adsorption and swelling experiments were not measured simultaneously (Meehan, 1927; Robertson and Christiansen, 2005) or performed on exactly the same coal samples (Ottiger et al., 2008). Other authors presented simultaneous *in situ* adsorption and swelling results but the volumetric strain was extrapolated from a local measurement – using strain gauges (Levine, 1996; Harpalani and Schraufnagel, 1990; Battistutta et al., 2010) or LVDT sensors (Chen et al., 2012; Espinoza et al., 2014) – or by monitoring the silhouette expansion (Day et al., 2008). Perrier et al. (2017) presented an experimental setup providing simultaneous *in situ* measurements of both adsorption and deformation for the same sample in the exact same conditions, which can be directly used for model validation. Gas adsorption measurements are performed using a custom-built manometric apparatus and deformation measurements are performed using a digital image correlation set-up. This set-up allows full-field displacement measurements, which may be crucial for heterogeneous, anisotropic or cracked samples.

As far as modeling is concerned, molecular simulations are the classical tools at the nanoscale. Important efforts have been involved in molecular simulations in order to characterise adsorption-induced deformation in nanoporous materials (Vandamme et al., 2010; Brochard et al., 2012a; Hoang and Galliero, 2015) and these investigations showed on few configurations that pressures applied on the pore surfaces may be very high (few hundred of MPa), depending on the thermodynamic conditions and on the pore sizes. Note that an alternative approach based on a non-local density functional theory can be used to obtain highly resolved evolutions of pore pressure *versus* pore widths and bulk pressure in slit-shaped pores for a large spectrum of thermodynamic conditions on the whole range of micropore widths, even for complex fluids (Grégoire et al., 2018). However, if macroscopic adsorption isotherms may be reconstructed in a consistent way from molecular simulations through the material pore size distribution (Khaddour et al., 2014), molecular simulation tools are not tractable to predict resulting deformation at a macroscale due to the fluid confinement in nanopores (pore sizes below 2 *nm*). Note that Kulasinski et al. (2017) proposed a molecular dynamic study where macroscopic swelling may be reconstructed from water adsorption in mesoporous wood (pore sizes in $[4-10]$ nm). If adsorption is essentially controlled by the amount and size of the pores, the mechanical effect of the pressure build up inside the pores due to fluid confinement requires some additional description about the topology and spatial organization of the porous network which is not easy to characterize, for sub-nanometric pores especially. Such a result motivates the fact that swelling is usually related to the adsorption isotherms instead of the pore pressure directly, the mechanical effect of the pore pressure being hidden in the poromechanical description.

In this context, different enhanced thermodynamical or poromechanical frameworks have been proposed within the last ten years to link adsorption, induced deformation and permeability changes (e.g Pan and Connell (2007);

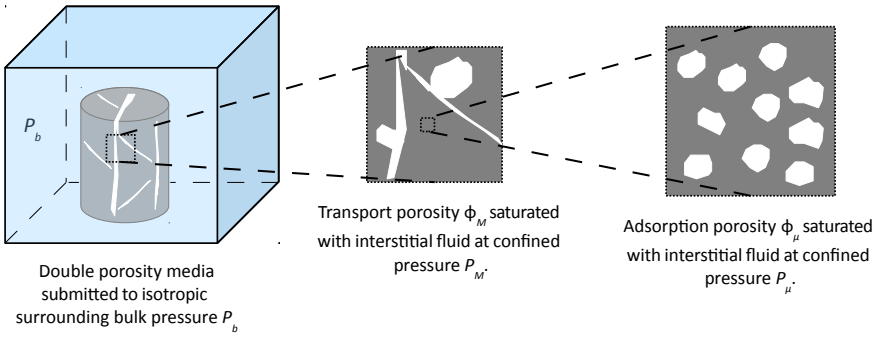

Figure 1: Schematic of a double porosity media.

Pijaudier-Cabot et al. (2011); Brochard et al. (2012b); Vermorel and Pijaudier-Cabot (2014); Perrier et al. (2015); Nikoosokhan et al. (2014)). For instance, Brochard et al. (2012b) (resp. Vermorel and Pijaudier-Cabot (2014)) proposed enhanced poromechanical frameworks where swelling volumetric deformation may be estimated as a function of the bulk pressure and a coupling (resp. a confinement) coefficient, which may be deduced from adsorption measurements. However, if these models are consistent with experimental results from the literature, they cannot be considered as truly predictive because the model parameters have to be identified to recover the experimental loading path. An incremental poromechanical framework with varying porosity has been proposed by Perrier et al. (2015) allowing the full prediction of the swelling induced by adsorption for isotropic nano-porous solids saturated with a single phase fluid, in reversible and isothermal conditions. This single porosity model has been compared with experimental data obtained by Ottiger et al. (2008) on bituminous coal samples filled with pure CH_4 and pure CO_2 at $T = 45^o$C and a fair agreement was observed for these low porosity coals but these types of models have to be enhanced to take into account the intrinsic double porosity features of such materials.

This study aims at characterizing the influence of an adsorbed phase on the instantaneous deformation of micro-to-macro porous media presenting distinct and well separated porosities in term of pore size distribution. A model accounting for double porosity is proposed and validated by in-situ and simultaneous experimental comparisons. The novelty of the approach is to propose an extended poromechanical framework taking into account the intrinsic double porosity features of such materials capable of predicting adsorption-induced swelling for high porous materials without any fitting parameters.

1. An incremental poromechanical framework with varying porosity for double porosity media

In this section, an incremental poromechanical framework with varying porosity proposed by Perrier et al. (2015) for single porosity media is extended to double porosity media.

We consider here a double porosity medium with distinct and separated porosities. The small porosity is called *adsorption porosity* (ϕ_μ) and the larger one *transport porosity* (ϕ_M). This medium is considered as isotropic with a linear poro-elastic behaviour and it is immersed and saturated by a surrounding fluid at bulk pressure P_b under isothermal conditions. Confinement effects may change the thermodynamic properties of the interstitial fluids in both porosities. The adsorption porosity is saturated by an interstitial fluid of density ρ_μ at pressure P_μ. The transport porosity is fully saturated by an interstitial fluid (single-phase) of density ρ_M at pressure P_M (see Fig. 1).

For saturated isotropic porous solids, in reversible and isothermal conditions and under small displacement-gradient assumptions, classical poromechanics may be rewritten for double porosity media Coussy (2004) :

$$
\begin{aligned}
d\tilde{G}_s &= d\Psi_s + dW_s && (1)\\
&= \underbrace{\sigma_{ij} : d\varepsilon_{ij} + P_M d\phi_M + P_\mu d\phi_\mu}_{d\Psi_s} + \underbrace{d(-P_M\phi_M - P_\mu\phi_\mu)}_{dW_s} && (2)\\
&= \sigma_{ij} : d\varepsilon_{ij} - \phi_M dP_M - \phi_\mu dP_\mu \, . && (3)
\end{aligned}
$$

In Eq. 1–3, $(\tilde{G}_s, \Psi_s, W_s)$ are respectively the Gibbs free energy, the Helmholtz free energy and the mechanical work of the skeleton. The state variables $(\varepsilon_{ij}, \phi_M, \phi_\mu)$ are respectively the infinitesimal strain tensor, the transport porosity and the adsorption porosity. The associated thermodynamical forces $(\sigma_{ij}, P_M, P_\mu)$ are respectively the Cauchy stress tensor and the fluid pore pressures in both porosities.

For an isotropic linear poro-elastic medium, the state equations are then given by:

$$\left\{\begin{array}{rcl} \sigma_{ij} & = & \frac{\partial \tilde{G}_s}{\partial \varepsilon_{ij}} \\ \phi_M & = & -\frac{\partial \tilde{G}_s}{\partial P_M} \quad , \qquad \text{and then:} \\ \phi_\mu & = & -\frac{\partial \tilde{G}_s}{\partial P_\mu} \end{array}\right. \tag{4}$$

$$\left\{\begin{array}{rcl} d\sigma & = & K(\phi_M,\phi_\mu)d\varepsilon - b_M(\phi_M,\phi_\mu)dP_M - b_\mu(\phi_M,\phi_\mu)dP_\mu \\ d\phi_M & = & b_M(\phi_M,\phi_\mu)d\varepsilon + \frac{dP_M}{N_{MM}(\phi_M,\phi_\mu)} - \frac{dP_\mu}{N_{M\mu}(\phi_M,\phi_\mu)} \\ d\phi_\mu & = & b_\mu(\phi_M,\phi_\mu)d\varepsilon - \frac{dP_M}{N_{\mu M}(\phi_M,\phi_\mu)} + \frac{dP_\mu}{N_{\mu\mu}(\phi_M,\phi_\mu)} \end{array}\right. .$$

In Eq. 4, $(\sigma = \sigma_{kk}/3)$ and $(\varepsilon = \varepsilon_{kk})$ are respectively the total mean stress and the volumetric strain. $(K, b_M, b_\mu, N_{MM}, N_{M\mu}, N_{\mu M}, N_{\mu\mu})$ are respectively the apparent modulus of incompressibility and six poromechanical properties, which depends on the two evolving porosities ϕ_M and ϕ_μ and on the constant skeleton matrix modulus.

Considering a single cylindrical porosity[2], homogenization models Halpin and Kardos (1976) yield to:

$$\left\{\begin{array}{lll} K(\phi) = \frac{K_s G_s(1-\phi)}{G_s + K_s\phi} & , & G_s = \frac{3K_s(1-2\nu_s)}{2(1+\nu_s)} \\ b(\phi) = 1 - \frac{K(\phi)}{K_s} & , & N(\phi) = \frac{K_s}{b(\phi)-\phi} \end{array}\right. . \tag{5}$$

In Eq. 5, ϕ is the porosity and (G_s, ν_s) are respectively the shear modulus and the Poisson ratio of the skeleton matrix.

Practically and for high porosity media, an iterative process of homogenization is chosen to avoid discrepancies in the apparent properties estimation as noticed by Barboura (2007). The iterative process of homogenization for a cylindrical porosity is detailed in Appendix A. Full details on the iterative processes for both spherical and cylindrical porosities are presented in Perrier et al. (2015).

Considering that the two porosities are distinct, well separated and both cylindrical, the iterative process can be used in two successive steps to determine the different modulus of incompressibility. Note that this two step homogenization process may be reversed as well to estimate the skeleton properties knowing the apparent ones:

$$\begin{array}{rcl} (K,G) & = & \mathcal{F}_n\left(\mathcal{F}_n(K_s,G_s,\phi_\mu),\phi_M\right) \\ \text{and } (K_s,G_s) & = & \mathcal{R}_n(\mathcal{R}_n(K,G,\phi_M),\phi_\mu)\ . \end{array} \tag{6}$$

In Eq. 6, $(\mathcal{F}_n, \mathcal{R}_n)$ stand as the standard and the reverse iterative processes of homogenization defined in Eq. A.1 and A.2 respectively. K_s and G_s (resp. K and G) are the skeleton (resp. apparent) incompressible and shear modulii.

Based on stress/strain partitions (Coussy, 2004) and on the response of the medium saturated by a non-adsorbable

[2]This assumption is discussed in Perrier et al. (2015) where both spherical and cylindrical porosities are considered.

fluid (Nikoosokhan et al., 2013), the six poromechanical properties ($b_M, b_\mu, N_{MM}, N_{M\mu}, N_{\mu M}, N_{\mu\mu}$) may be identified:

$$\left\{\begin{array}{c} b_M = 1 - \frac{K}{K_\mu} \quad , \quad b_\mu = K(\frac{1}{K_\mu} - \frac{1}{K_s}) \\ \\ \frac{1}{N_{MM}} = \frac{b_M - \phi_M}{K_\mu} \quad , \quad \frac{1}{N_{M\mu}} = \frac{1}{N_{\mu M}} = (b_M - \phi_M)(\frac{1}{K_\mu} - \frac{1}{K_s}) \quad , \\ \\ \frac{1}{N_{\mu\mu}} = \frac{(b_\mu - \phi_\mu)}{K_s} + (b_M - \phi_M)(\frac{1}{K_\mu} - \frac{1}{K_s}) \end{array}\right. \tag{7}$$

$$\text{with} \quad K_\mu = \mathcal{F}_n(K_s, G_s, \phi_\mu) \, .$$

For a porous medium saturated by a fluid under isothermal conditions (isotropic surrounding/bulk pressure: P_b, density: ρ_b), $d\sigma = -dP_b$ and Eq. 4 yield to:

$$\left\{\begin{array}{rcl} d\varepsilon & = & \frac{-dP_b}{K_s} \\ \\ d\phi_M & = & \frac{-\phi_M}{K_s} dP_b \\ \\ d\phi_\mu & = & \frac{-\phi_\mu}{K_s} dP_b \end{array}\right. . \tag{8}$$

Therefore, classical poromechanics predicts a shrinkage of the porous matrix and a decrease of the porosity under bulk pressure. This has been confirmed by experimental measurements (e.g. Reucroft and Patel (1986) on a natural coal with a non-adsorbable gas).

Considering that the fluid is confined within both porosities, the thermodynamic properties (pressures: P_M, P_μ, densities: ρ_M, ρ_μ) of the interstitial fluid in the two porosities (ϕ_M, ϕ_μ) differ from the surrounding ones (P_b, ρ_b) but the thermodynamic equilibrium imposes that the three fluids are chemically balanced (equality of the chemical potentials μ_b, μ_M and μ_μ). Assuming that the Gibbs-Duhem equation ($dP = \rho d\mu$) still applies for both the surrounding fluid and the interstitial ones, a macroscopic relation between the interstitial pore pressures and the surrounding one may be derived similarly to the relation initially proposed by Vermorel and Pijaudier-Cabot (2014) and used in Perrier et al. (2015) for single porosity media:

$$\left\{\begin{array}{rcccl} dP_M & = & \rho_M \frac{dP_b}{\rho_b} & = & \frac{dP_b}{1-\chi_M} \\ \\ dP_\mu & = & \rho_\mu \frac{dP_b}{\rho_b} & = & \frac{dP_b}{1-\chi_\mu} \end{array}\right. . \tag{9}$$

In Eq. 9, ($\chi_M = 1 - \frac{\rho_b}{\rho_M}$) and ($\chi_\mu = 1 - \frac{\rho_b}{\rho_\mu}$) are the confinement degrees in the transport and in the adsorption porosities respectively, which characterize how confined is the interstitial fluid due to the number of adsorbate moles n_M^{ex} and n_μ^{ex} that exceeds the number of fluid moles at bulk conditions in porosities ϕ_M and ϕ_μ respectively:

$$\left\{\begin{array}{rcccl} \chi_M & = & \frac{n_M^{ex}}{n_M^{tot}} \quad \text{with} \quad n_M^{tot} & = & n_M^{ex} + \frac{\rho_b V_{\phi_M}}{M} \\ \\ \chi_\mu & = & \frac{n_\mu^{ex}}{n_\mu^{tot}} \quad \text{with} \quad n_\mu^{tot} & = & n_\mu^{ex} + \frac{\rho_b V_{\phi_\mu}}{M} \end{array}\right. . \tag{10}$$

In Eq. 10, (V_{ϕ_M}, V_{ϕ_μ}) are the connected porous volume corresponding to the transport porosity ϕ_M and to the adsorption porosities ϕ_μ respectively, n_M^{ex} and n_μ^{ex} are the number of adsorbate moles that exceeds the number of fluid moles at bulk conditions and n_M^{tot} and n_μ^{tot} are the total number of moles of interstitial fluid in porosities ϕ_M and ϕ_μ respectively. Generally, there is no way to link separately the two confinement degrees χ_M and χ_μ to quantities that can be measured experimentally because the partition of the excess number of adsorbate moles n^{ex}, which can be measured experimentally, within the two porosities is unknown ($n^{ex} = n_M^{ex} + n_\mu^{ex}$). However, assuming that the two scales of porosities are well separated, one can consider that most of the adsorption phenomenon occurs in the adsorption porosity ($n_\mu^{ex} >> n_M^{ex}$) and that the interstitial fluid is not confined in the transport porosity:

$$\left\{\begin{array}{rcccl} \chi_\mu & \approx & \frac{n^{ex}}{n_\mu^{tot}} \quad \text{and} \quad dP_\mu & = & \frac{dP_b}{1-\chi_\mu} \\ \\ \chi_M & \approx & 0 \quad \text{and} \quad dP_M & = & dP_b \end{array}\right. . \tag{11}$$

Finally, a new incremental poromechanical framework with varying porosities for double porosity media is proposed:

$$\begin{cases} d\varepsilon &= (\frac{b_\mu}{1-\chi_\mu} + b_M - 1)\frac{dP_b}{K} \\ d\phi_\mu &= \left[\underbrace{\left(\frac{b_\mu}{1-\chi_\mu} + b_M - 1 \right) \frac{b_\mu}{K}}_{T_1} + \underbrace{\frac{1}{N_{\mu\mu}\left(1-\chi_\mu\right)}}_{T_2} - \underbrace{\frac{1}{N_{\mu M}}}_{T_3} \right] dP_b \\ d\phi_M &= \left[\underbrace{\left(\frac{b_\mu}{1-\chi_\mu} + b_M - 1 \right) \frac{b_M}{K}}_{T_4} - \underbrace{\frac{1}{N_{\mu M}\left(1-\chi_\mu\right)}}_{T_5} + \underbrace{\frac{1}{N_{MM}}}_{T_6} \right] dP_b \\ \chi_\mu &= \frac{n^{ex}}{n_\mu^{tot}} \quad \text{with} \quad n_\mu^{tot} = n^{ex} + \frac{\rho_b V_{\phi_\mu}}{M} = n^{ex} + \frac{m_s}{M}\frac{\rho_b}{\rho_s}\frac{\phi_\mu}{1-\phi_\mu-\phi_M} \end{cases} \tag{12}$$

In Eq. 12, $K(\phi_M, \phi_\mu)$ is given by Eq. 6, $(b_M, b_\mu, N_{MM}, N_{\mu M}, N_{\mu\mu})$ all depend on (ϕ_M, ϕ_μ) and are given by Eq. 7, (n^{ex}, P_b, ρ_b) are experimentally measurable and (m_s, M, ρ_s) are respectively the adsorbent sample mass, the molar mass of the adsorbed gas and the density of the material composing the solid matrix of the porous adsorbent.

2. Validation by experimental comparisons on a double porosity synthetic activated carbon

The experimental results obtained by Perrier et al. (2017) on a double porosity synthetic activated carbon (*Chemviron*) are used in this study for validation purpose. The main advantage of the proposed method is to provide simultaneous *in situ* measurements of both adsorption and deformation for the same sample in the exact same conditions.

The material and the adsorption-induced strain measurements are briefly recalled in section 2.1. The model input parameters are identified in section 2.2 and finally comparisons between experimental and model results are performed in section 2.3.

2.1. Material description and adsorption-induced strain measurements

In this section, the experimental results obtained by Perrier et al. (2017) on a double porosity synthetic activated carbon are briefly recalled. Full details may be found in Perrier et al. (2017).

An activated carbon (*Chemviron*) is used as adsorbent material. The sample is a cylinder and its main characteristics are collected in Table 1. The geometrical dimensions have been measured with a caliper, the mass has been measured with a *Precisa* scale (XT 2220 M-DR), the specific pore surface has been measured with a gas porosimeter (*Micromeretics* ASAP 2020) according to the BET theory (Brunauer et al., 1938). The specific micropore volume has been estimated according to the IUPAC classification (Thommes et al., 2015) (pore diameter below 2 nm) based on a pore size distribution deduced from a low-pressure adsorption isotherm (N_2 at 77 K from 8.10^{-8} to 0.99 P/P_0 in relative pressure range) measured with the same gas porosimeter according to the HK theory (Horvath and Kawazoe, 1983). The specific macropore volume has been estimated according to the IUPAC classification (Thommes et al., 2015) (pore diameter above 50 nm) based on a pore size distribution deduced from mercury intrusion porosimetry. Both porosimetry techniques show that there are almost no pore of diameters between 2 nm and 50 nm in this material. The two porosities are well separated in term of pore size distribution.

The adsorbates, CO_2 and CH_4, as well as the calibrating gas, *He*, are provided with a minimum purity of 99.995%, 99.995% and 99.999% respectively.

Table 1: Main characteristics of the adsorbent and the adsorbates.

Property	Unit	Symbol	Value
Height	(cm)	h	1.922 ± 0.004
Diameter	(cm)	d	2.087 ± 0.002
Volume	(ml)	V_{ech}	6.57 ± 0.03
Adsorbent sample mass	(g)	m_s	4.137 ± 0.001
Solid matrix density	(kg/L)	ρ_s	2.4 ± 0.8
Specific pore surface	($m^2.g^{-1}$)	S_{BET}	1090 ± 10
Specific micropore volume	($cm^3.g^{-1}$)	v_{ϕ_μ}	0.51 ± 0.01
Adsorption porous volume	(cm^3)	V_{ϕ_μ}	2.115 ± 0.001
Adsorption porosity	(%)	ϕ_μ^0	32 ± 1
Specific macropore volume	($cm^3.g^{-1}$)	v_{ϕ_M}	0.66 ± 0.01
Transport porous volume	(cm^3)	V_{ϕ_M}	2.712 ± 0.001
Transport porosity	(%)	ϕ_M^0	41 ± 1
Total porosity	(%)	ϕ^0	73 ± 2
CO_2 molar mass	($g.mol^{-1}$)	$M_{\mathrm{CO_2}}$	44.01
CH_4 molar mass	($g.mol^{-1}$)	$M_{\mathrm{CH_4}}$	16.04

CO_2 and CH_4 excess adsorption isotherms are built step by step from gas adsorption measurements performed using a custom-built manometric set-up. Simultaneously adsorption-induced swelling strain are measured based on digital image correlation. Full details are provided in Perrier et al. (2017).

Fig. 3 presents the results of these simultaneous measurements for an activated carbon filled with pure CO_2 and pure CH_4 at $T = 318.15$ K and $T = 303.15$ K respectively. Full-field deformation maps and collected experimental data are reported in Perrier et al. (2017).

Fig. 3.a presents the results in term of excess adsorption/desorption isotherms. CO_2 and CH_4 gas sorption in activated carbon is a reversible phenomenon and no hysteresis is observed between adsorption and desorption paths as previously reported in the literature in Khaddour et al. (2014). Noting that adsorbed quantity amount increases when temperature decreases, Fig. 3.a shows that CO_2 is preferentially adsorbed in carbon compare to CH_4 as previously reported in the literature (Ottiger et al., 2008; Battistutta et al., 2010). This is the reason why CO_2 injection is used to increase CH_4 recovery in Enhanced Coal Bed Methane production.

Fig. 3.b presents the results in term of adsorption-induced volumetric strain. CO_2 and CH_4 gas adsorption-induced deformation is a reversible phenomenon but a small hysteresis is observed between the adsorption and the desorption paths. This hysteresis is not linked to the adsorption-deformation couplings but is due to an elastic compaction of the carbon matrix grains (Perrier, 2015). Cycling effect and material compaction are detailed in (Perrier et al., 2017). For a given pressure, CO_2 adsorption produces more volumetric deformation than CH_4 adsorption, which is the source of the rapid decrease in CO_2 injectivity during coal bed methane production enhanced by CO_2 injection.

2.2. Identification of model input parameters

The input parameters of the incremental poromechanical framework with varying porosities for double porosity media presented in Eq. (12) are:

- The adsorbent sample mass (m_s), the molar mass of the adsorbed gas (M_{CO_2}, M_{CH_4}), the density of the material composing the solid matrix of the porous adsorbent (ρ_s), the initial transport porosity (ϕ_M^0) and the initial adsorption porosity (ϕ_μ^0), which are all given in Table 1.

- The surrounding fluid bulk pressure (P_b), the excess adsorbed quantities (n^{ex}) and the bulk density (ρ_b), which are both experimentally measured or deduced. From the experimental measurements of the excess adsorption isotherm (Fig. 3.a), a power-law fit is identified and used as an input in the incremental estimation of Eq. (12). From the bulk pressure and the temperature, the bulk density (ρ_b) of the surrounding fluid is estimated by its state equation using the AGA8 software (Starling, 1994).

- The skeleton incompressibility (K_s) and shear (G_s) modulii are deduced from the apparent ones from the two step homogenization reversed process presented in Eq. (6). The apparent properties are experimentally measured using an ultra-sonic technique where longitudinal and transverse waves are generated by a piezo-electric source and detected by a laser Doppler vibrometer (Shen et al., 2016):

$$\left\{ \begin{array}{rcl} K & = & \rho_s(V_p^2 - \frac{4}{3}V_s^2) \\ G & = & \rho_s V_s^2 \end{array} \right. . \tag{13}$$

  In Eq. 13, (V_p, V_s) are respectively the velocities of the longitudinal and the transverse waves. With $V_p = (302 \pm 2)$ m.s^{-1} and $V_s = (176 \pm 1)$ m.s^{-1}, we get $K = (120 \pm 15)$ MPa and $G = (75 \pm 8)$ MPa and then $K_s = (6.0 \pm 0.6)$ GPa and $G_s = (3.5 \pm 0.4)$ GPa.

  Note that the experimental technique developed by Perrier et al. (2017) and allowing simultaneous measurements of adsorption-induced swelling may also be used to characterize K_s directly as previously reported by Hol and Spiers (2012). Indeed, if a non-adsorbable gas (such as helium) is used, the skeleton incompressible modulus may be deduced from bulk pressure and volumetric shrinkage strain measurements using Eq. 8. Figure 2 presents a typical result of K_s direct identification. An experimental value of $K_s = (6 \pm 1)$ GPa is then obtained, which is in good agreement with the latter one. Note that dynamic and static mechanical properties may differ

for a lot of materials so a perfect match is not expected here. However, for this material with a low rigidity, the difference between the static and the dynamic properties is relatively not important and it may stand within the measurement uncertainty.

As discussed in Perrier et al. (2017), activated carbon is subjected to cycling effect and material compaction. The process to produce the active carbon is composed of three phases: first the carbon is grinded, then it is activated, and finally it is compacted to obtain a cylindrical sample. During the first cycle of gas adsorption, there is a competition between the grain compaction shrinkage and the adsorption-induced volumetric swelling and a large hysteresis is observed because of the material compaction. This compaction is mostly irreversible and after the first cycle, the second and the third cycles are reversible. Fig. 3 presents the results in term of adsorption-induced volumetric strain obtained during the third cycle when the activated carbon is fully compacted and swelling strain fully reversible. The two other cycles are presented in Perrier et al. (2017). However, the ultra-sonic technique used to identify the apparent elastic properties has been performed on the sample before compaction and the skeleton elastic properties may differ after compaction. Therefore, a second direct K_s identification has been performed after the adsorption-induced swelling test and the value of $K_s = 7.0 \pm 0.8$ GPa is obtained. Assuming that the shear skeleton modulus is affected by the compaction in the same proportion of the incompressible one – *i.e.* assuming that the Poisson's ratio is not affected by the compaction – the following skeleton modulii are identified and further used in the comparisons with experimental data:

$$\left\{ \begin{array}{rcl} K_s & = & (7.0 \pm 0.8) \text{ GPa} \\ G_s & = & (4.1 \pm 0.4) \text{ GPa} \end{array} \right. . \tag{14}$$

2.3. Comparisons between experimental and model results

Fig. 3 presents also the results obtained with the double porosity adsorption-induced deformation model presented in part 1. All the parameters being identified in section 2.2, the volumetric strain induced by gas adsorption is estimated step by step as well as the evolutions of the transport and adsorption porosities and the poromechanical properties without any fitted parameters.

Fig. 3.b shows that the double porosity adsorption-induced deformation model presented in part 1 is capable to predict swelling induced by both CH_4 and CO_2 gas adsorption without any additional fitting parameters. The entry parameters in the model are those collected in Table 1, the skeleton elastic modulii corrected as explained in the latter section, and the adsorption isotherms. For this activated carbon, a swelling strain of $\approx 2\%$ is recovered for a CO_2 bulk pressure up to 46 bar and a swelling strain of $\approx 1.5\%$ is recovered for a CH_4 bulk pressure up to 107 bar.

Fig. 4 shows the same results in term of excess adsorption quantities versus adsorption-induced swelling. One can note that the relationship between excess adsorbed quantities and resulting swelling is not linear. Moreover, the two evolutions for the two different gases are close together showing that the volumetric swelling is directly linked to the excess adsorbed quantity.

Fig. 5 shows that for this challenging high micro and macro porous activated carbon, a single porosity model, as the one presented in Perrier et al. (2015), highly overestimates the swelling deformation induced by gas adsorption in this activated carbon. The coupling appearing between the evolving adsorption porosity and the evolving transport porosity limits the macroscopic swelling of the material. This can only be captured with a double porosity model.

2.4. Evolution of the poromechanical properties under free swelling

The proposed double porosity model being validated by experimental comparisons in the latter section, we study here the evolution of the poromechanical properties under this free swelling.

Fig. 6 presents the evolution of the confinement degree in the adsorption porosity under free swelling for an activated carbon filled with pure CO_2 and pure CH_4 at $T = 318.15$ K and $T = 303.15$ K respectively. At the early adsorption stage, the confinement degree is high (≥ 0.9) for both CO_2 and CH_4. This is due to the fact that at the onset of adsorption, the interstitial fluid density is much higher that the bulk density ($\rho_b << \rho_\mu$). Upon swelling,

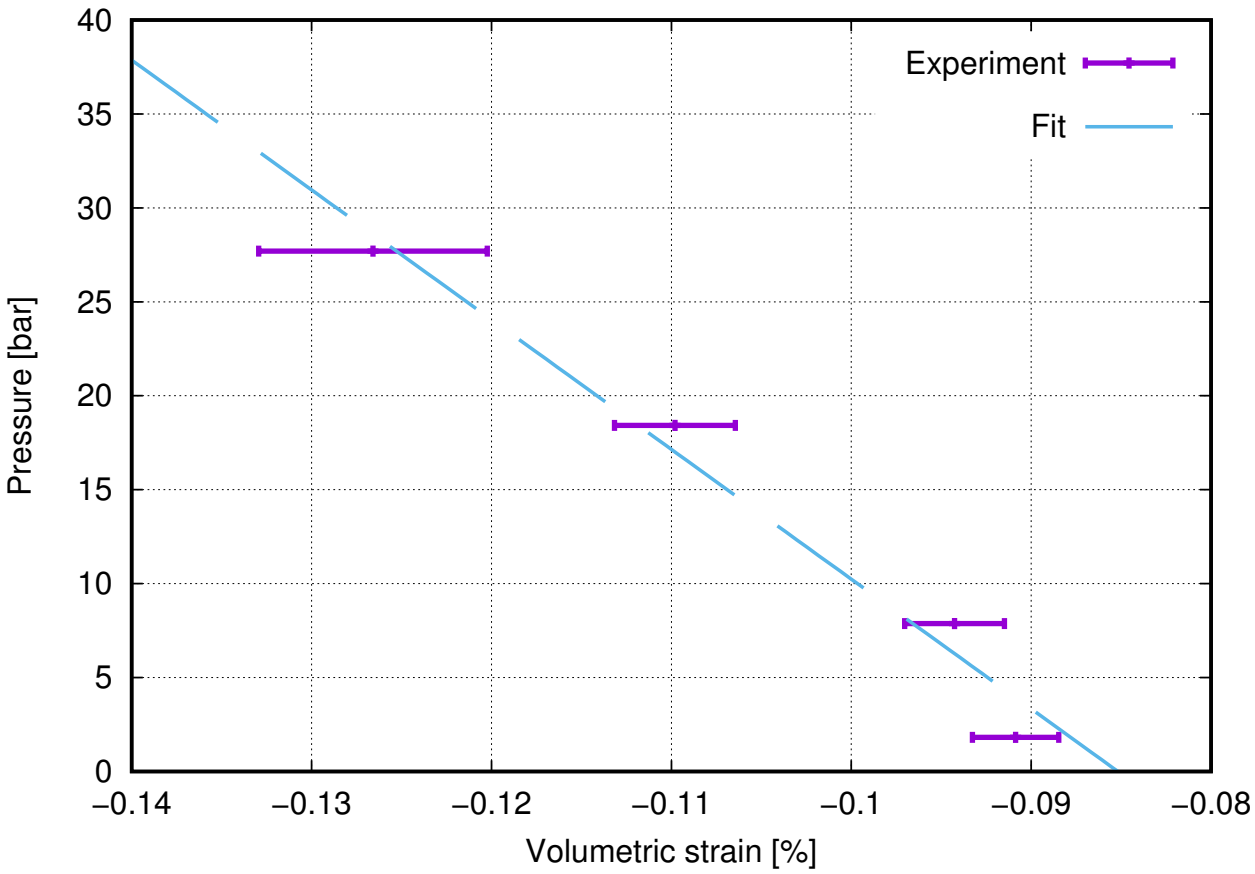

Figure 2: Activated carbon K_s direct identification based on Eq. 8 thanks to helium bulk pressure and volumetric shrinkage strain measurements (the slope provides directly K_s).

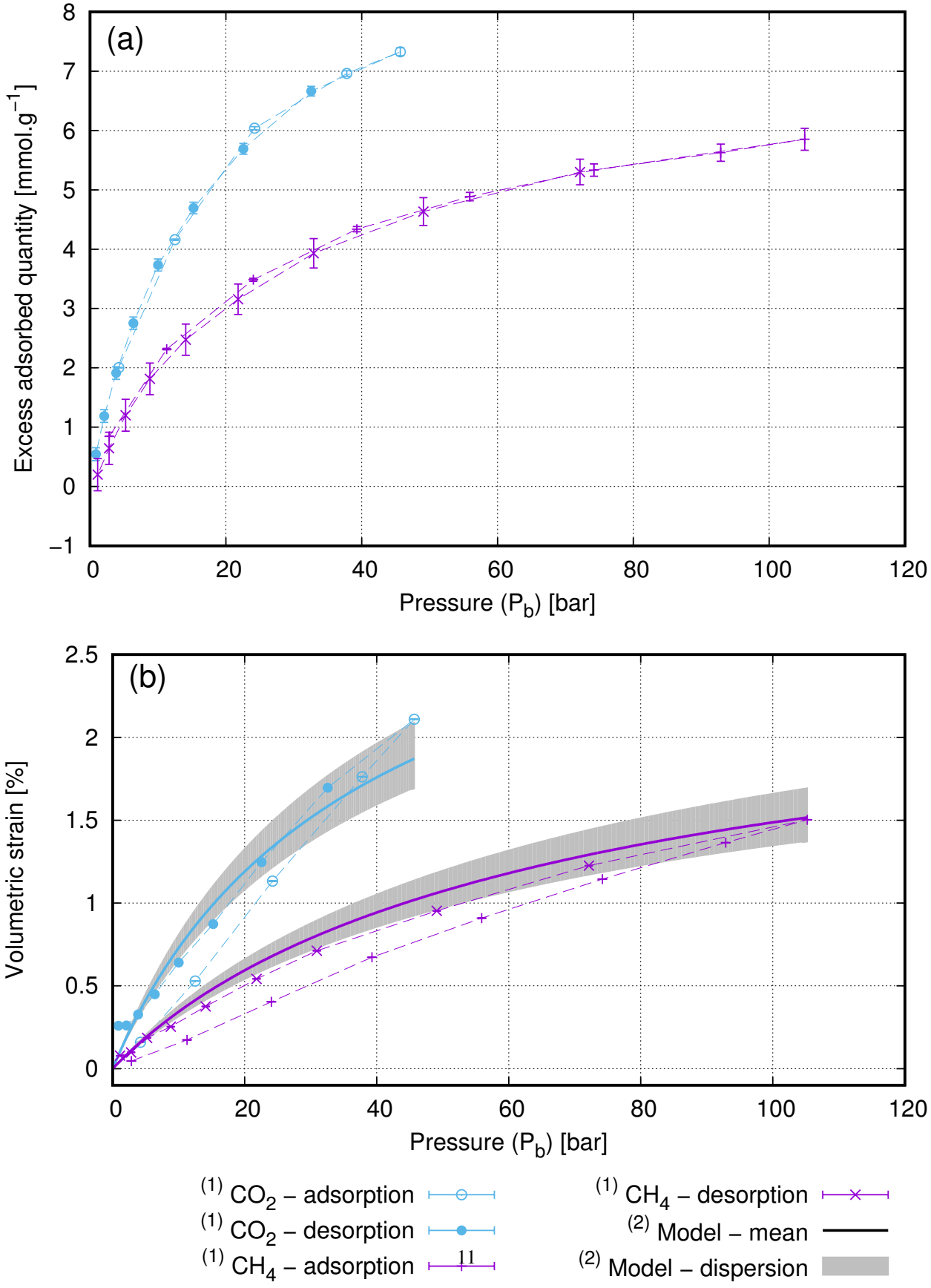

(1) Experiment (Perrier et al., 2017), (2) Model (this study).

Figure 3: Simultaneous adsorption and induced swelling measurements for an activated carbon filled with pure CO_2 and pure CH_4 at T = 318.15 K and T = 303.15 K respectively: (a) experimental excess adsorption isotherms; (b) comparison between experimental and modeling adsorption-induced swelling results.

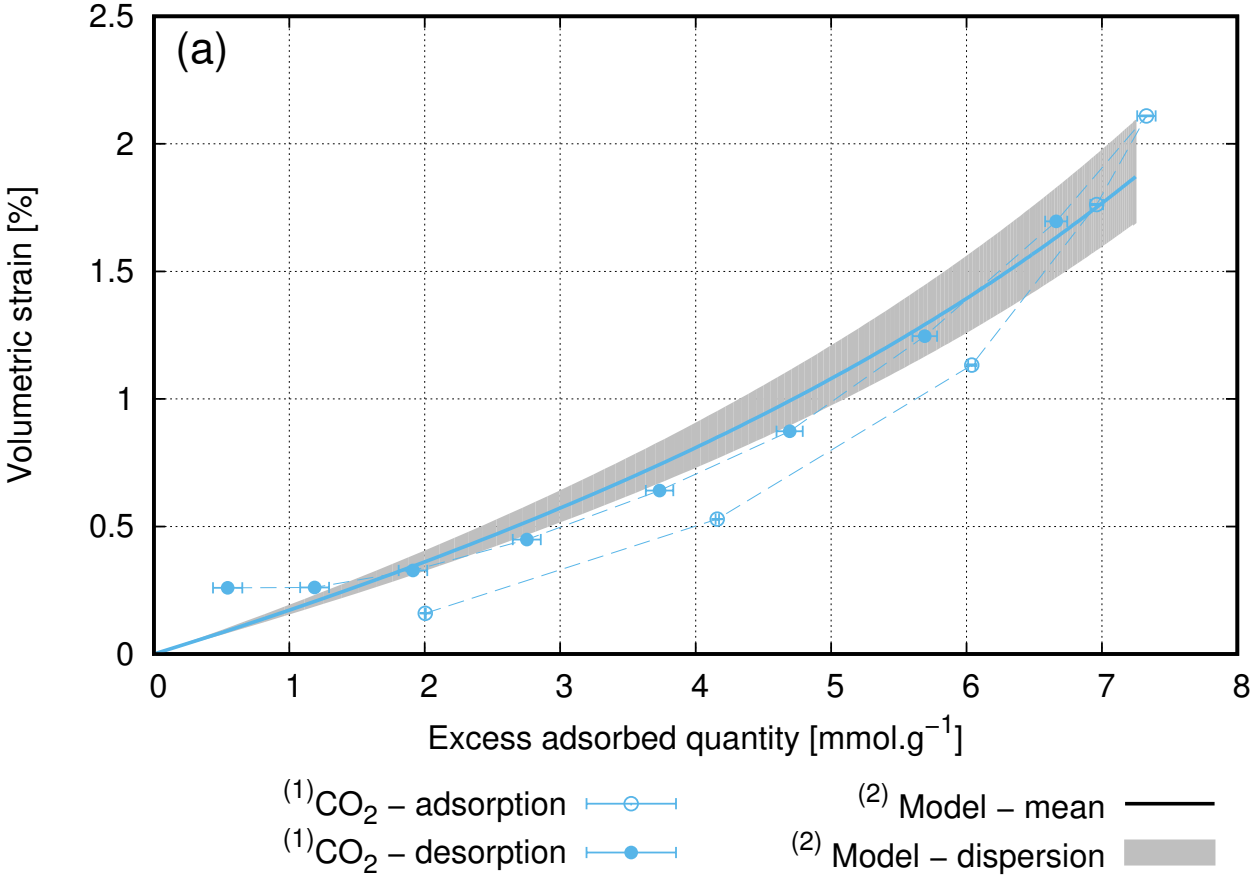

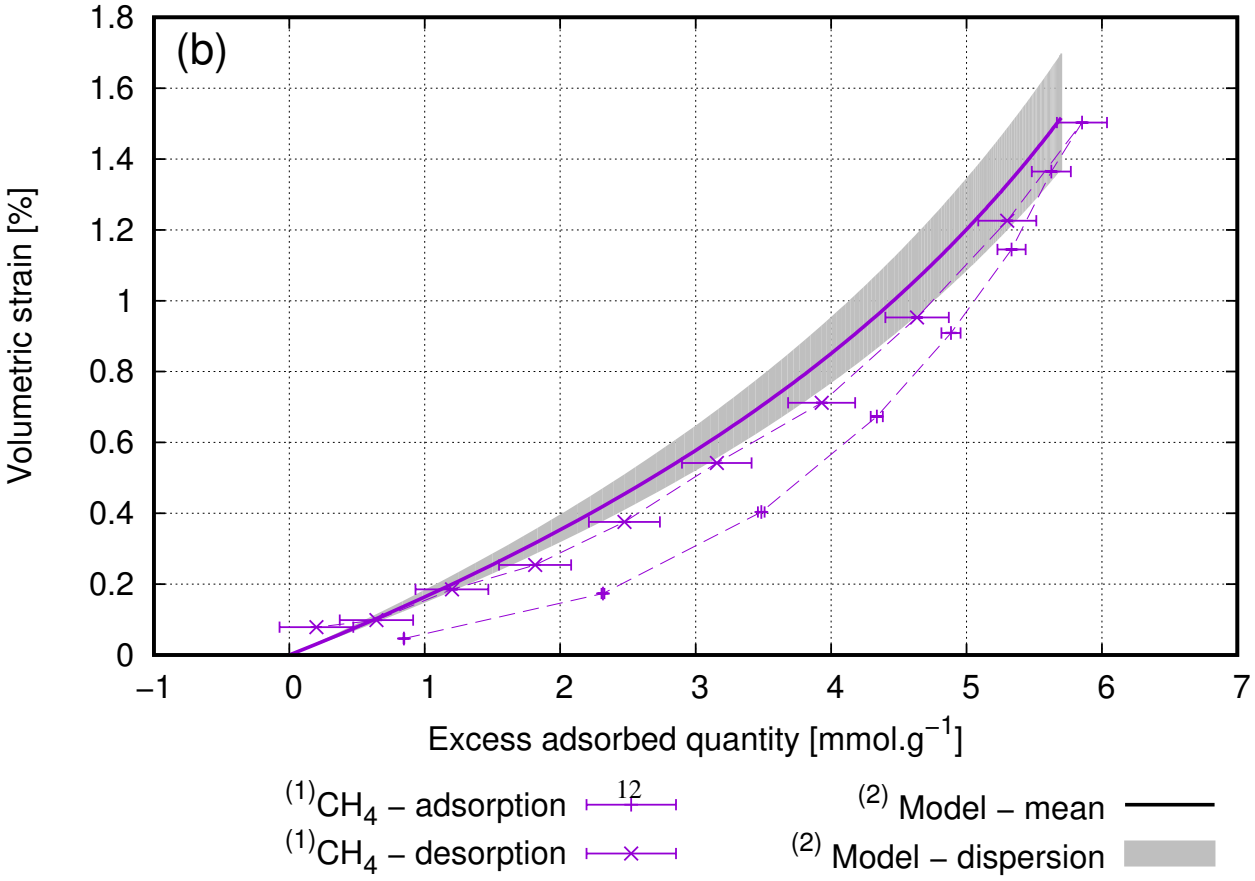

$^{(1)}$ Experiment (Perrier et al., 2017), $^{(2)}$ Model (this study).

Figure 4: Comparison between experimental and modeling results in term of excess adsorption quantities versus adsorption-induced swelling for an activated carbon: (a) CO_2 at T = 318.15 K; (b) CH_4 at T = 303.15 K.

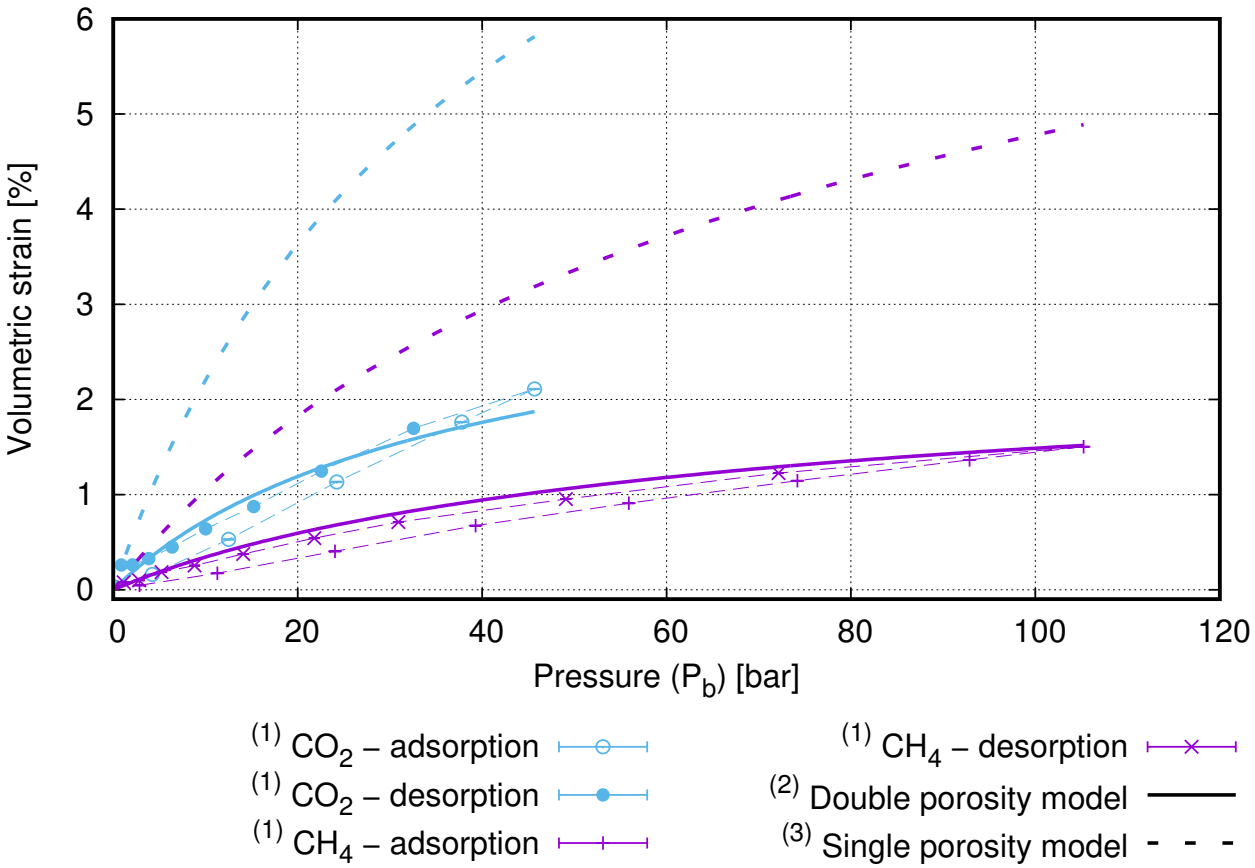

(1) Experiment (Perrier et al., 2017), (2) Model (this study),
(3) Model (Perrier et al., 2015).

Figure 5: Comparison between the adsorption-induced swelling results provided by the single and the double porosity models for an activated carbon filled with pure CO_2 and pure CH_4 at T = 318.15 K and T = 303.15 K respectively.

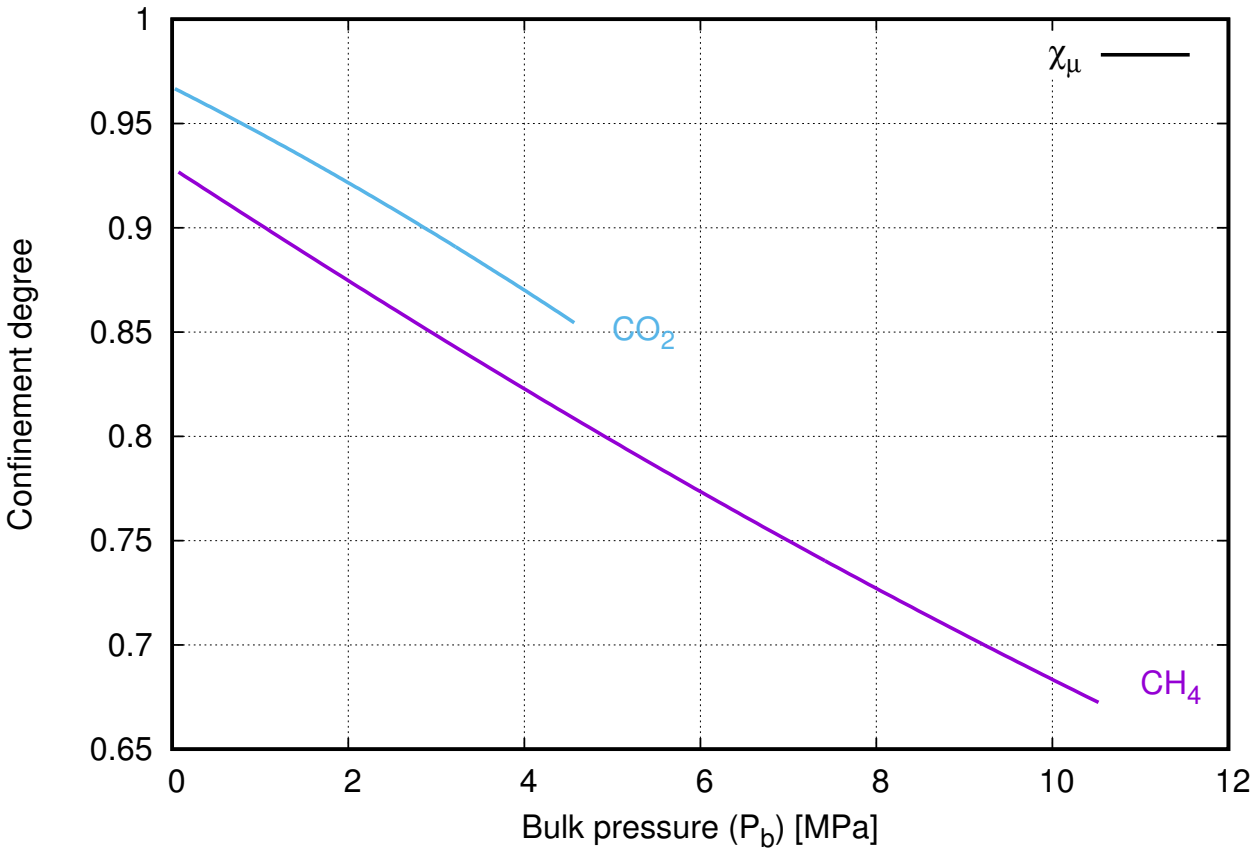

Figure 6: Evolution of the confinement degree in the adsorption porosity (χ_μ) under free swelling for an activated carbon filled with pure CO_2 and pure CH_4 at $T = 318.15$ K and $T = 303.15$ K respectively.

the confinement degree is decreasing for both CO_2 and CH_4. This may due to two main reasons: firstly, the ratio of the bulk density over the interstitial fluid density is increasing; secondly, the adsorption porosity is increasing due to the active carbon swelling, and therefore, the confinement of the fluid decreases. That way the functional $\frac{\phi_\mu}{1-\phi_\mu-\phi_M}$ in Eq. 12 is increasing even faster. Therefore the total number of adsorbed gas moles increases faster than the excess number of moles and the confinement degree is decreasing, the CO_2 interstitial fluid being more confined than the CH_4 one.

Figs. 7 presents the evolution of the poromechanical properties in term of relative variations under free swelling. Fig. 7.a shows that all porosities are increasing with increasing bulk pressure under free swelling and, for this activated carbon, a relative variation of total porosity of $\approx 2\%$ is recovered for a CO_2 bulk pressure up to 46 bar and a a relative variation of $\approx 1.5\%$ is recovered for a CH_4 bulk pressure up to 107 bar. Due to the increase of porosities, Fig. 7.b shows that incompressible modulii are decreasing under free swelling, K decreasing faster than K_μ. Consequently, b_M is increasing and b_μ upon free swelling as shown in Fig. 7.c. The evolution of the coupling poromechanical properties $N_{MM}, N_{\mu\mu}, N_{\mu M}$ are more difficult to anticipate but Fig. 7.d shows that they are all decreasing upon swelling.

Even if it may be counter-intuitive, Fig. 7.a shows that, under free swelling, the transport porosity is not decreasing even if the adsorption porosity increases. It simply increases less than the adsorption porosity. Note that this cannot be generalised for other materials or thermodynamic conditions because this is due to the complex couplings appearing between the transport and the adsorption porosities in Eq. 12. For the conditions considered here, Fig. 8 shows that, whatever the bulk pressure, the different contributions of the terms (T_1 to T_6) in Eq. 12 lead to a positive derivative of both porosities in respect to the bulk pressure, and therefore both porosities increases upon swelling (see Eq. 12 for T_1 to T_6 term expressions).

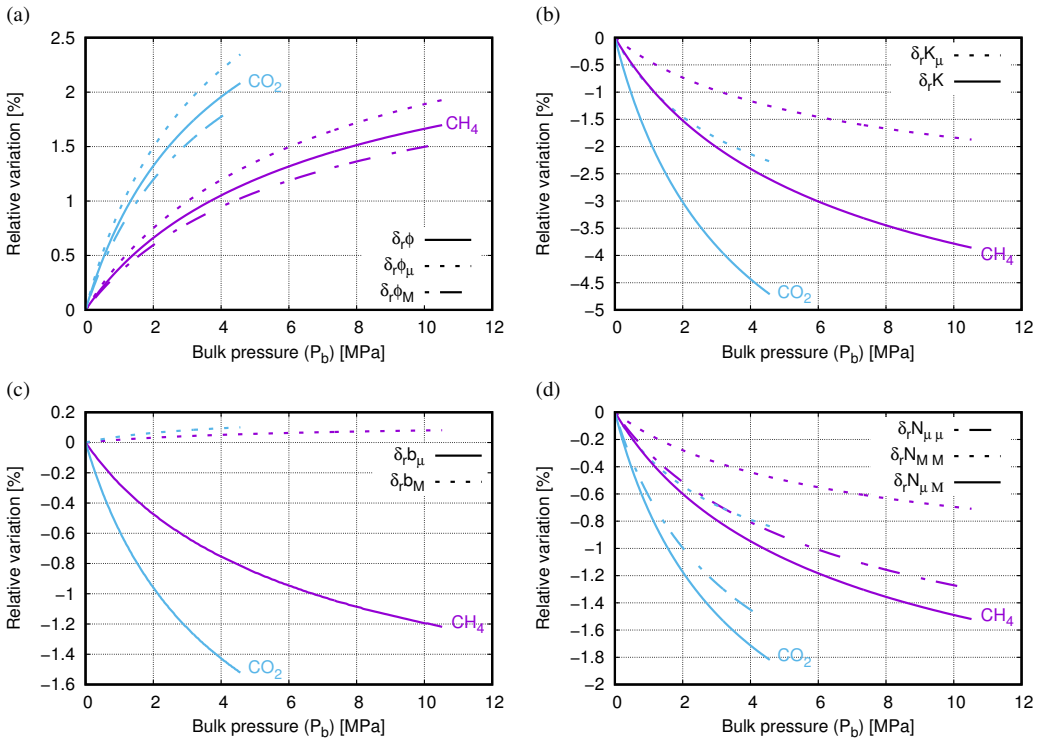

where $\delta_r X = \frac{X - X^0}{X^0}$ is the relative variation of X.

Figure 7: Evolution of the poromechanical properties in term of relative variations under free swelling for an activated carbon filled with pure CO_2 and pure CH_4 at $T = 318.15$ K and $T = 303.15$ K respectively.

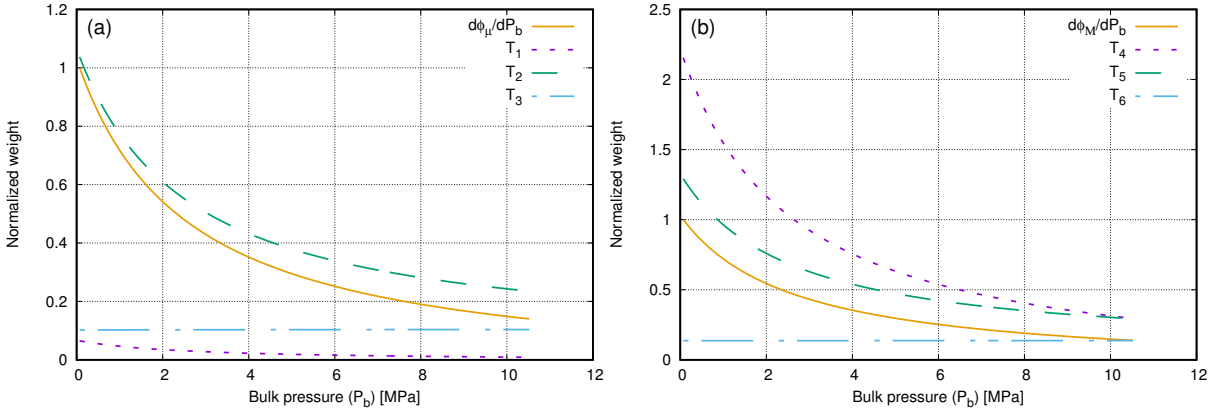

Figure 8: Relative contribution of the terms (T_1 to T_6) in the derivative of adsorption (ϕ_μ) and transport (ϕ_M) porosities in respect to the bulk pressure (see Eq. 12 for T_1 to T_6 term expressions). Normalized weight are estimated in respect to the derivative initial values.

3. Case-study of constrained swelling

In this section, one case-study of constrained swelling is considered. The volumetric strain is then assumed to be equal to zero and Eq. 12 may be rewritten as:

$$\begin{cases} d\varepsilon &= 0 \\ d\phi_\mu &= \left(\underbrace{\frac{1}{N_{\mu\mu}\left(1-\chi_\mu\right)}}_{T_7} - \underbrace{\frac{1}{N_{\mu M}}}_{T_8} \right) dP_b \\ d\phi_M &= \left(\underbrace{-\frac{1}{N_{\mu M}\left(1-\chi_\mu\right)}}_{T_9} + \underbrace{\frac{1}{N_{MM}}}_{T_{10}} \right) dP_b \\ \chi_\mu &= \frac{n^{ex}}{n_\mu^{tot}} \quad \text{with} \quad n_\mu^{tot} = n^{ex} + \frac{\rho_b V_{\phi_\mu}}{M} = n^{ex} + \frac{m_s}{M}\frac{\rho_b}{\rho_s}\frac{\phi_\mu}{1-\phi_\mu-\phi_M} \end{cases} \tag{15}$$

Figs. 9 presents the evolution of the poromechanical properties in term of relative variations under constrained swelling. Fig. 9.a shows that the total porosity and the transport porosity are now decreasing whereas the adsorption porosity still increases. Indeed, and for the conditions considered here, Fig. 10 shows that, whatever the bulk pressure, T_7 and T_8 in Eq. 15 lead to a positive derivative of the adsorption porosity in respect to the bulk pressure, whereas T_9 and T_{10} in Eq. 15 lead to a negative derivative of the transport porosity. Figs. 9.b to 9.d show the corresponding evolution of the other poromechanical properties with increasing bulk pressure. Fig. 11 shows the evolution of the total mean stress under constraint swelling. The volumetric strain being imposed equal to zero, the continuum is submitted to compressive total mean stresses.

Concluding remarks

- A new incremental poromechanical framework with varying porosity has been proposed allowing the prediction of the swelling induced by adsorption. Within this framework, the adsorption-induced strain are incrementally estimated based on experimental adsorption isotherm measurements only. The evolution of the porosity and the evolutions of the poromechanical properties, such as the apparent incompressible modulus, the apparent shear modulus, the Biot modulus and the Biot coefficient, are also predicted by the model.

- A double porosity model has been proposed for which the adsorption porosity and the transport porosity are distinguished. These two scales of porosity are supposed to be well separated and a two steps homogenization process is used to estimate incrementally the evolution of the poromechanical properties, which couple the evolutions of both porosities.

- An existing custom-built experimental set-up has been used to test the relevance of this double porosity model. A challenging high micro and macro porous activated carbon has been chosen for this purpose. An adsorption porosity of 32.2±0.2% and a transport porosity of 41.6±0.2% have been characterized as well as its apparent and skeleton elastic properties. *In situ* adsorption-induced swelling has been measured for pure CO_2 and pure CH_4 at $T = 318.15$ K and $T = 303.15$ K respectively and the corresponding model responses have been estimated. It has been shown that the double porosity model is capable to predict accurately the swelling induced by both CH_4 and CO_2 gas adsorption without any fitting parameters. Conversely, it has been shown that a single porosity model highly overestimates the swelling deformation induced by gas adsorption for this high micro and macro porous activated carbon. The coupling appearing between the evolving adsorption porosity and the evolving

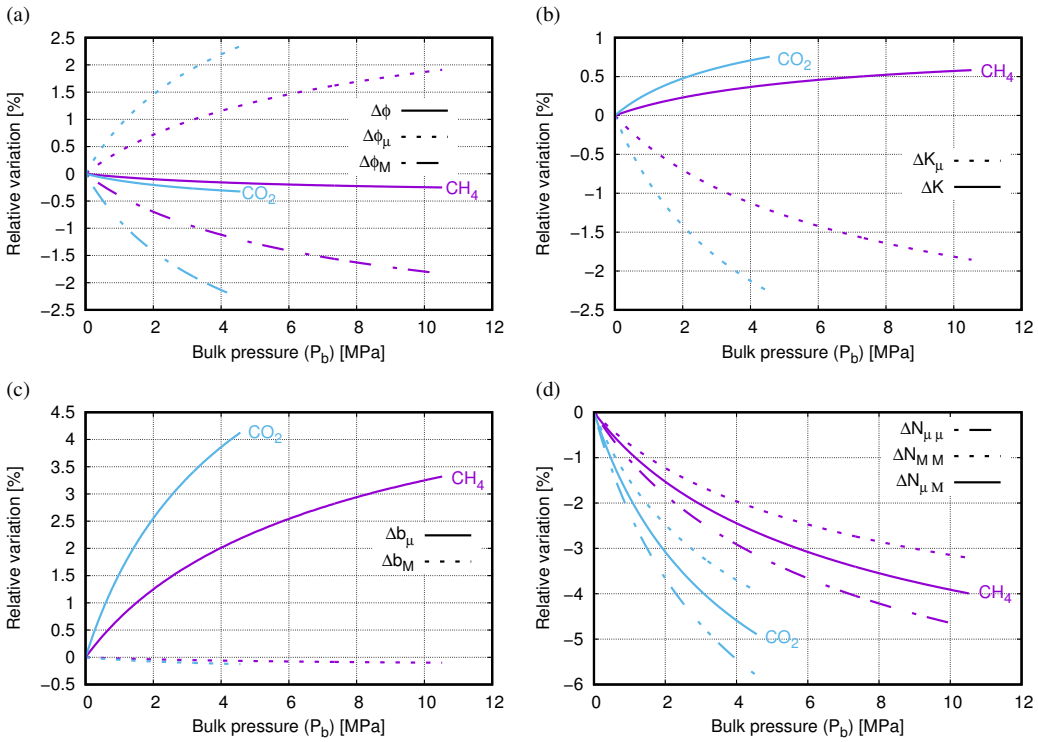

where $\delta_r X = \frac{X - X^0}{X^0}$ is the relative variation of X.

Figure 9: Evolution of the poromechanical properties in term of relative variations under constrained swelling for an activated carbon filled with pure CO_2 and pure CH_4 at $T = 318.15$ K and $T = 303.15$ K respectively.

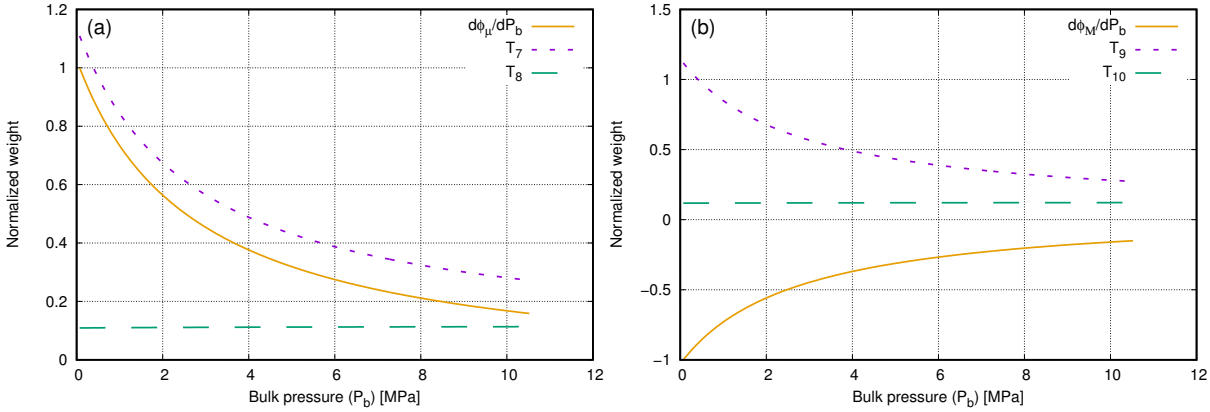

Figure 10: Relative contribution of the terms (T_7 to T_{10}) in the derivative of adsorption (ϕ_μ) and transport (ϕ_M) porosities in respect to the bulk pressure (see Eq. 15 for T_7 to T_{10} term expressions). Normalized weight are estimated in respect to the derivative initial values.

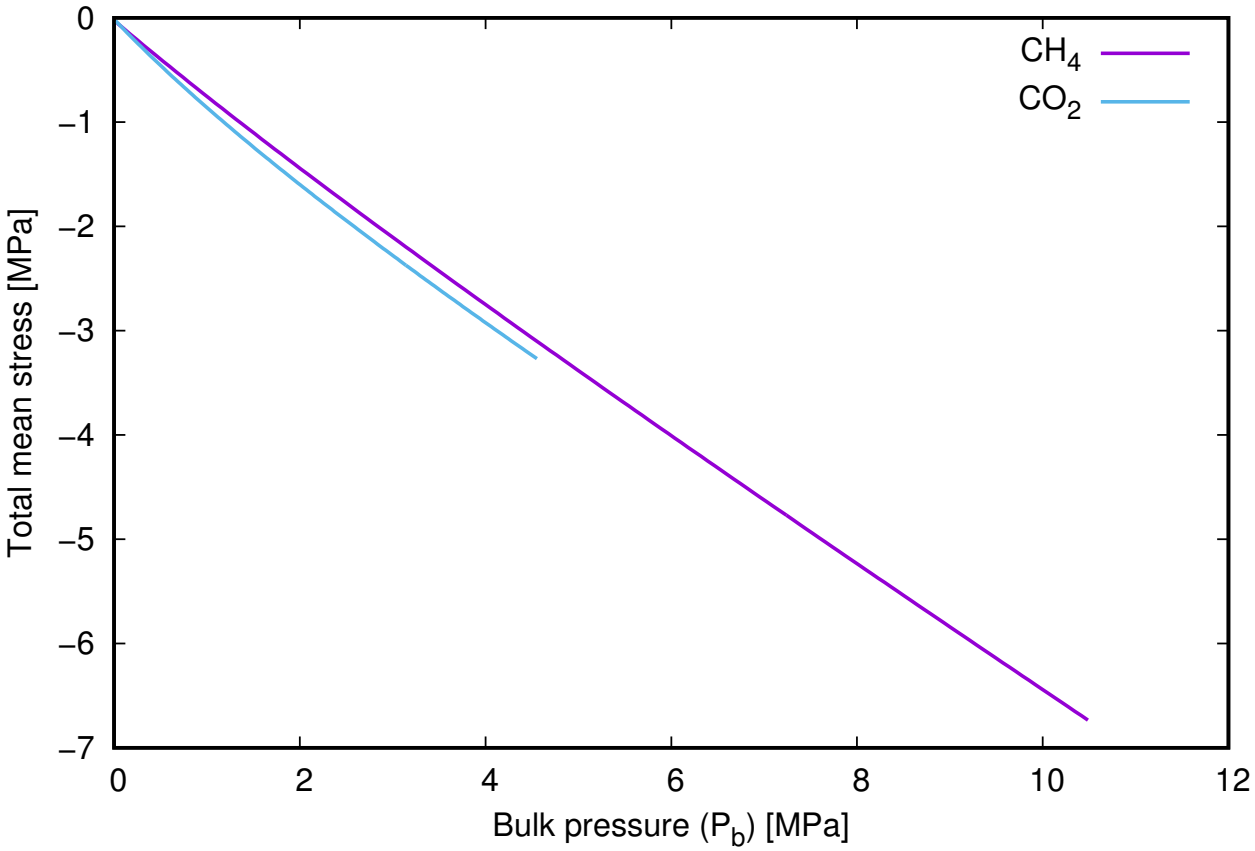

Figure 11: Total mean stress evolution under constrained swelling.

transport porosity limits the macroscopic swelling of the material. This can only be captured with a double porosity model.

- After validation, the double porosity model has been used to discuss the evolution of the poromechanical properties under free and constraint swelling. The case-study of constraint swelling consists here in assuming a global volumetric strain equal to zero. It has been shown that for the considered material, all porosities are increasing with increasing bulk pressure under free swelling, whereas the total porosity and the transport porosity are decreasing when the adsorption porosity still increases under constraint swelling.

Acknowledgements

Financial supports from the *Région Aquitaine* through the grant CEPAGE (20121105002), from the *Conseil Départemental 64* through the grant CEPAGE2 (2015_0768), from the *Insitut Carnot* ISIFoR and from the *Université de Pau et des Pays de l'Adour* through the grant Bonus Qualité Recherche are gratefully acknowledged. We also gratefully acknowledge Dr. Frédéric Plantier and Dr. Christelle Miqueu for their advices and our different discussions and Dr. Valier Poydenot for his help concerning the ultra-sonic technique and the apparent properties identification. D. Grégoire and G. Pijaudier-Cabot are fellows of the Institut Universitaire de France.

Appendix A. Iterative process of homogenization

Following Smaoui-Barboura Barboura (2007), an iterative homogenization process may be applied for the linear homogenization functions used for a cylindrical porosity (Eq. 5)[3].

Considering a given cylindrical porosity ϕ, the local skeleton properties (K_s, G_s) and a given number of increment n, the global homogenized properties (K_m, G_m) are determined step by step using the following scheme:

$$
\begin{array}{rcl}
(K_m, G_m) & = & \mathcal{F}_n(K_s, G_s, \phi) \quad \text{with:} \\
\left[\begin{array}{l}
K^{(0)} = K_s \quad , \quad G^{(0)} = G_s \quad , \quad \Delta\phi = \frac{\phi}{n} \quad , \quad \phi^{(i)} = \frac{\Delta\phi}{1-\phi+i\Delta\phi} \\
\left\{\begin{array}{rcl} K^{(i)} & = & \mathcal{H}_K(\phi^{(i)}, K^{(i-1)}, G^{(i-1)}) \\ G^{(i)} & = & \mathcal{H}_G(\phi^{(i)}, K^{(i-1)}, G^{(i-1)}) \end{array}\right. \\
K_m = K^{(n)} \quad , \quad G_m = G^{(n)}
\end{array}\right. & , & \qquad \text{(A.1)} \\
\text{where:} \left\{\begin{array}{rcl} \mathcal{H}_K(\phi, K_s, G_s) & = & K_s - \frac{\phi K_s}{1-(1-\phi)\times(\frac{K_s}{K_s+G_s})} \\ \mathcal{H}_G(\phi, K_s, G_s) & = & G_s - \frac{\phi G_s}{1-(1-\phi)\times(\frac{K_s+2G_s}{2K_s+2G_s})} \end{array}\right. & . &
\end{array}
$$

Moreover, the latter iterative process may be reversed to determine step by step the local skeleton properties

[3] For a full description on the iterative processes for both spherical and cylindrical porosities see Perrier et al. (2015).

(K_s, G_s) knowing the homogenized properties (K_m, G_m) and a given number of increment n:

$$
\begin{array}{rcl}
(K_s, G_s) & = & \mathcal{R}_n(K_m, G_m, \phi) \quad \text{with:} \\
\left[\begin{array}{l}
K^{(0)} = K_m \quad , \quad G^{(0)} = G_m \quad , \quad \Delta\phi = \frac{\phi}{n} \quad , \quad \phi^{(i)} = \frac{\Delta\phi}{1-\phi+i\Delta\phi} \\
\left\{ \begin{array}{rcl}
K^{(i)} & = & \mathcal{H}_K(\phi^{(i)}, K^{(i-1)}, G^{(i-1)}) \\
G^{(i)} & = & \mathcal{H}_G(\phi^{(i)}, K^{(i-1)}, G^{(i-1)})
\end{array} \right. \\
K_s = K^{(n)} \quad , \quad G_s = G^{(n)}
\end{array} \right. & , & \qquad (A.2) \\
\text{where:} \left\{ \begin{array}{rcl}
\mathcal{H}_K(\phi, K_s, G_s) & = & K_s + \frac{\phi K_s}{1-(1-\phi)\times(\frac{K_s}{K_s+G_s})} \\
\mathcal{H}_G(\phi, K_s, G_s) & = & G_s + \frac{\phi G_s}{1-(1-\phi)\times(\frac{K_s+2G_s}{2K_s+2G_s})}
\end{array} \right. & . &
\end{array}
$$

Bibliography

Barboura, S. S., 2007. Modélisation micromécanique du comportement de milieux poreux non linéaires : Applications aux argiles compactées. Ph.D. thesis, Université Pierre et Marie Curie.

Battistutta, E., Van Hemert, P., Lutynski, M., Bruining, H., Wolf, K.-H., 2010. Swelling and sorption experiments on methane, nitrogen and carbon dioxide on dry selar cornish coal. International Journal of Coal Geology 84 (1), 39–48.

Biot, M. A., 1941. General theory of three-dimensional consolidation. Journal of Applied Physics 12 (2), 155–164.

Briggs, H., Sinha, R. P., 1933. Expansion and contraction of coal caused respectively by the sorption and discharge of gas. Proceedings of the Royal Society of Edinburgh 53, 48–53.

Brochard, L., Vandamme, M., Pellenq, R. J., Fen-chong, T., 2012a. Adsorption-induced deformation of microporous materials: Coal swelling induced by C02-CH4 competitive adsorption. Langmuir 28 (5).

Brochard, L., Vandamme, M., Pellenq, R.-M., 2012b. Poromechanics of microporous media. Journal of the Mechanics and Physics of Solids 60 (4), 606–622.

Brunauer, S., Emmett, P. H., Teller, E., 1938. Adsorption of Gases in Multimolecular Layers. Journal of the American Chemical Society 60 (2), 309–319.

Chen, G., Yang, J., Liu, Z., 2012. Method for simultaneous measure of sorption and swelling of the block coal under high gas pressure. Energy & Fuels 26 (7), 4583–4589.

Coussy, O., 2004. Poromechanics. John Wiley & Sons, Ltd.

Day, S., Fry, R., Sakurovs, R., 2008. Swelling of australian coals in supercritical co2. International Journal of Coal Geology 74 (1), 41–52.

Espinoza, D., Vandamme, M., Pereira, J.-M., Dangla, P., Vidal-Gilbert, S., 2014. Measurement and modeling of adsorptive-poromechanical properties of bituminous coal cores exposed to co2: Adsorption, swelling strains, swelling stresses and impact on fracture permeability. International Journal of Coal Geology 134, 80–95.

Gor, G. Y., Huber, P., Bernstein, N., feb 2017. Adsorption-induced deformation of nanoporous materials - A review. Applied Physics Reviews 4 (1), 11303.

Grégoire, D., Malheiro, C., Miqueu, C., 2018. Estimation of adsorption-induced pore pressure and confinement in a nanoscopic slit pore by a density functional theory. Continuum Mech. Thermodyn., in press.

Halpin, J. C., Kardos, J. L., 1976. The Halpin-Tsai Equations: A Review. Polymer Engineering & Science 16 (5), 344–352.

Harpalani, S., Schraufnagel, R. A., 1990. Influence of matrix shrinkage and compressibility on gas production from coalbed methane reservoirs'. In: SPE Annual Technical Conference and Exhibition. Society of Petroleum Engineers, pp. 171–179.

Hoang, H., Galliero, G., 2015. Couplings between swelling and shear in saturated slit nanopores : A molecular simulation study. Physical Review E 91 (012401), 1–9.

Hol, S., Spiers, C. J., 2012. Competition between adsorption-induced swelling and elastic compression of coal at co 2 pressures up to 100mpa. Journal of the Mechanics and Physics of Solids 60 (11), 1862–1882.

Horvath, G., Kawazoe, K., 1983. Method for the calculation of effective pore size distribution in molecular sieve carbon. Journal of Chemical Engineering of Japan 16 (6), 470–475.

Khaddour, F., Knorst-Fouran, A., Plantier, F., Piñeiro, M. M., Mendiboure, B., Miqueu, C., 2014. A fully consistent experimental and molecular simulation study of methane adsorption on activated carbon. Adsorption 20 (4), 649–656.

Kulasinski, K., Derome, D., Carmeliet, J., 2017. Impact of hydration on the micromechanical properties of the polymer composite structure of wood investigated with atomistic simulations. Journal of the Mechanics and Physics of Solids 103 (Supplement C), 221 – 235.

Larsen, J. W., 2004. The effects of dissolved CO2 on coal structure and properties. International Journal of Coal Geology 57 (1), 63–70.

Levine, J. R., 1996. Model study of the influence of matrix shrinkage on absolute permeability of coal bed reservoirs. Geological Society, London, Special Publications 109 (1), 197–212.

Meehan, F. T., 1927. The Expansion of Charcoal on Sorption of Carbon Dioxide. Proceedings of the Royal Society A: Mathematical, Physical and Engineering Sciences 115 (770), 199–207.

Nikoosokhan, S., Brochard, L., Vandamme, M., Dangla, P., Pellenq, R. J.-M., Lecampion, B., Fen-Chong, T., 2013. CO2 Storage in Coal Seams: Coupling Surface Adsorption and Strain. John Wiley & Sons, Inc., Ch. 7, pp. 115–132.

Nikoosokhan, S., Vandamme, M., Dangla, P., 2014. A poromechanical model for coal seams saturated with binary mixtures of ch4 and co2. Journal of the Mechanics and Physics of Solids 71 (Supplement C), 97 – 111.

Ottiger, S., Pini, R., Storti, G., Mazzotti, M., 2008. Competitive adsorption equilibria of co2 and ch4 on a dry coal. Adsorption 14 (4-5), 539–556.

Pan, Z., Connell, L., 2007. A theoretical model for gas adsorption-induced coal swelling. International Journal of Coal Geology 69 (4), 243–252.

Perrier, L., 2015. Coupling between adsorption and deformation in microporous media. Ph.D. thesis, Université Pau & Pays Adour.

Perrier, L., Pijaudier-Cabot, G., Grégoire, D., 2015. Poromechanics of adsorption-induced swelling in microporous materials: a new poromechanical model taking into account strain effects on adsorption. Continuum Mechanics and Thermodynamics 27 (1), 195–209.

Perrier, L., Plantier, F., Grégoire, D., 2017. A novel experimental set-up for simultaneous adsorption and induced deformation measurements in microporous materials. Review of Scientific Instruments 88 (3).

Pijaudier-Cabot, G., Vermorel, R., Miqueu, C., Mendiboure, B., 2011. Revisiting poromechanics in the context of microporous materials. Comptes Rendus Mécanique 139 (12), 770–778.

Pini, R., Ottiger, S., Burlini, L., Storti, G., Mazzotti, M., 2009. Role of adsorption and swelling on the dynamics of gas injection in coal. Journal of Geophysical Research: Solid Earth (1978–2012) 114 (B4).

Reucroft, P., Patel, H., 1986. Gas-induced swelling in coal. Fuel 65 (6), 816–820.

Robertson, E. P., Christiansen, R. L., 2005. Measuring and modeling sorption-induced coal strain. In: 4th Annual Conference on Carbon Capture and Sequestration. US DOE NETL, pp. 1–16.

Sampath, K., Perera, M., Ranjith, P., Matthai, S., Rathnaweera, T., Zhang, G., Tao, X., 2017. Ch4co2 gas exchange and supercritical co2 based hydraulic fracturing as cbm production-accelerating techniques: A review. Journal of CO2 Utilization 22 (Supplement C), 212 – 230.

Shen, C., Brito, D., Poydenot, V., Diaz, J., Garambois, S., Bordes, C., Oct. 2016. Seismic wave propagation in heterogeneous limestone samples. In: Journées d'Etude des Milieux Poreux. Anglet, France, pp. 1–2.

Sing, K., Everett, D., Haul, R., Moscou, L., Pierotti, R., Rouquerol, J., Siemieniewska, T., 1985. Reporting physisorption data for gas/solid systems with special reference to the deter- mination of surface area and porosity. Pure and Applied Chemistry 57 (4), 603–619.

Starling, K. E., 1994. Compressibility and super compressibility for natural gas and other hydrocarbon gases. Tech. Rep. AGA Report NO.8, Transmission Measurement Committee Report.

Thommes, M., Cychosz, K. a., 2014. Physical adsorption characterization of nanoporous materials: Progress and challenges. Adsorption 20, 233–250.

Thommes, M., Kaneko, K., Neimark, A. V., Olivier, J. P., Rodriguez-Reinoso, F., Rouquerol, J., Sing, K. S. W., 2015. Physisorption of gases, with special reference to the evaluation of surface area and pore size distribution (IUPAC Technical Report). Pure and Applied Chemistry 87 (9-10), 1051–1069.

Vandamme, M., Brochard, L., Lecampion, B., Coussy, O., 2010. Adsorption and strain: The CO2-induced swelling of coal. Journal of the Mechanics and Physics of Solids 58 (10), 1489–1505.

Vermorel, R., Pijaudier-Cabot, G., 2014. Enhanced continuum poromechanics to account for adsorption induced swelling of saturated isotropic microporous materials. European Journal of Mechanics-A/Solids 44, 148–156.